Force generation in dividing E. coli cells: A handles-on approach using optical tweezers

Verhoeven, G.S.

Citation

Verhoeven, G. S. (2008, December 2). *Force generation in dividing E. coli cells: A handles-on approach using optical tweezers*. Retrieved from https://hdl.handle.net/1887/13301

VII

Chapter 7: Force-extension curves of DNA tethers attached to outer membrane protein OmpA in a living bacterium

Abstract

In this work, we characterize a system designed to study force generation during cell division in *Escherichia coli*. We present force-extension (F-x) curves of DNA tethers attached to a bacterial outer membrane protein (OmpA) in a living bacterium. The connection is made via a streptavidin-binding peptide SA-1, genetically inserted in a surface-displayed loop of the OmpA protein.

To separate the DNA compliance from bacterial compliance, the bacterial DNA tethers are compared with "pure" DNA tethers to an immobilized bead. We find that a height difference between the two DNA ends results in under-estimation of the force on the bead, due to what seems a substantial variation of the lateral trap stiffness along the axial direction.

Two variants of the OmpA were compared, one with C-terminal peptidoglycan (PG)-binding domain (*full-length*) and one without (β-*barrel*). For the bacterial DNA tethers, we find that tether lengths and F-x curves are similar to "pure" DNA F-x curves. In addition, for the truncated OmpA β-barrel, softer tethers are observed which could correspond to (short) membrane tubes. For the moment we cannot exclude that the observed variations are due to height variations between the tethers. However, for this construct, also two F-x curves were measured for which the tether length is much longer (6-7 μm) than the DNA contour length (2.16 μm). We speculate that these long tethers are membrane tubes, as the tethers displayed (partly) linear force-extension behavior with an effective spring constant of ~3 pN/μm.

Through the measurement of unbinding forces at two different pulling rates, we characterize the weakest bond in the molecular construct. We find unbinding forces that could correspond to the SA-1 peptide/streptavidin bond.

Introduction

Our aim is to tether an optically trapped bead to *Escherichia coli* and measure forces exerted on the outer membrane during growth and division of that bacterium (see also **Chapter 1**). The use of beads as handles to measure forces in biological processes is widespread. Beads can be attached to proteins, e.g. to study force generation by motor proteins such as kinesin (Visscher et al. 1999), or to measure forces of a growing microtubule (Kerssemakers et al. 2006). On the scale of cells, attached beads have been used to deform to red blood cells (Mills et al. 2004), or to pull membrane tubes from cells (Dai and Sheetz 1995) or lipid vesicles (Koster et al. 2005). Recently, it was demonstrated that through aspecific adhesion of beads on *E. coli* cells, membrane tubes can be pulled using optical tweezers (Jauffred et al. 2007).

Because we want to measure forces during the invagination of the cell, we cannot directly stick a bead onto a bacterium: the size of the bacterium (1 x 3 μm) and the bead (diameter: 2 μm) are similar. We need to tether the bead to an attachment point that is smaller than the scale of the invagination (~100 nm), which requires a spacer. We choose DNA, as it is (relatively) easy to manipulate, and its force-extension behavior is well known. Furthermore, there are many standard ways to attach a DNA molecule to a polystyrene bead.

The surface of an *Escherichia coli* bacterium consists of LPS (lipo-polysaccharide) molecules, and the surface-exposed parts of integral β-barrel proteins (Ruiz et al. 2006). Of these two components, β-barrels will likely withstand the highest forces before extraction. Furthermore, a β-barrel protein has a higher potential for mid-cell localization than an LPS molecule, by e.g. gene fusions in the periplasm (see **Chapters 4 and 5**).

How to tether a DNA molecule to the surface-exposed part of a β-barrel? We want a specific attachment, as only the β-barrel that localizes to mid-cell must be a target for binding. There are two obvious choices: Antibody-antigen and biotin-streptavidin. High-affinity biotinylated antibodies (such as the anti-FLAG M2 antibody) are commercially available. After genetic insertion of the corresponding epitope in one of the surface-exposed parts of the β-barrel, the antibody can bind to the β-barrel. For this approach, conformational restraining of a linear epitope might alter the affinity of the antibody (Giebel et al. 1995; Rice et al. 2006). A biotinylated DNA molecule can be attached to the antibody via streptavidin. Alternatively, the antibody can be covalently linked to the DNA,

however, this is technically more challenging (Cecconi et al. 2008).

It is also possible to biotinylate a β-barrel *in vivo* through genetic insertion of a specific peptide ("acceptor peptide"): an enzyme, biotin ligase, recognizes the acceptor peptide, and covalently adds a biotin molecule to it (Chapman-Smith and Cronan 1999). However, biotinylation in *Escherichia coli* occurs in the cytoplasm, and β-barrels are rapidly exported to the periplasm. Indeed, it was found that the efficiency of biotinylation of the β-barrel LamB was very low (Oddershede et al. 2002), and we want many attachment sites to be present.

A "hybrid" antigen-streptavidin alternative was recently described in a study that screened for peptides binding directly to streptavidin (Bessette et al. 2004). A peptide library was displayed in a surface-exposed loop of the OmpA β-barrel on the surface of *E. coli*, and high affinity binders to (among others) streptavidin were selected. A peptide was isolated (SA-1) that when present in β-barrel OmpA in *E. coli*, showed a thermal off-rate of ~ 10^{-3} s^{-1} (Bessette et al. 2004). For the experiments described in this chapter, OmpA containing this SA-1 peptide (cloned in our expression vector) is used (see also below).

Typical literature values for thermal off-rates for antibody-peptide bonds are 10^{-3}-10^{-4} s^{-1} (Deroo et al. 2008). For the unbinding of a FLAG-tagged protein (not constrained) from anti-FLAG antibody M2 (Sigma) a 10^{-5} s^{-1} thermal off-rate was reported (Nice et al. 1997). Compared to the commonly used biotin-streptavidin (thermal off-rate 10^{-6} s^{-1} (Piran and Riordan 1990)) the lifetime of an antibody-based bond under force will be shorter than that of biotin-streptavidin.

We can use the Bell model to estimate the lifetime of a bond under force. The model assumes that the off-rate depends exponentially on the applied force times a distance x_b (Bell 1978):

$$k_{off}(F) = k_{off}(0) \cdot e^{\frac{Fx_b}{k_bT}} \quad (\textbf{Equation 7.1})$$

The distance x_b can be interpreted as the distance a ligand has to be displaced "along the reaction coordinate" out of the binding pocket before it unbinds. Assuming a typical value for the barrier width (0.5 nm), antibody-peptide bonds are expected to be strong enough to withstand a force of a few pN for several minutes. Furthermore, by using multiple tethers, the load could be shared and higher forces can be exerted on the cell without breaking the molecular construct.
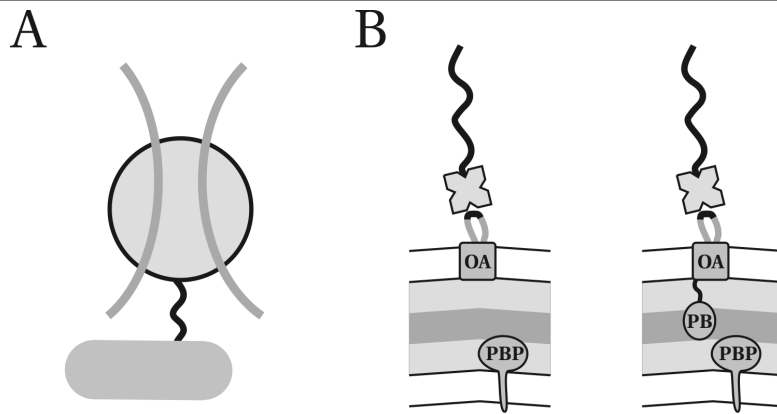
Figure 7.1. Schematic of the experiment: (A) An optically trapped DNA-coated bead is tethered to an immobilized bacterium. **(B)** Two molecular constructs are compared: the OmpA-177 β-barrel, without periplasmic domain (left), and the full-length OmpA protein, which contains an additional PG (peptidoglycan)-binding (PB) domain. The cell-wall synthesizing complexes are indicated with "PBP".

The protein fusions used in this chapter are depicted in **Figure 7.1**. Their construction and *in vivo* characterization is described in **Chapter 3**. A strain (MC1061) is used that either expresses OmpA-177^{SA-1} (the β-barrel) or OmpA^{SA-1}. This latter construct consists of the full-length OmpA protein, which includes an additional PG cell wall binding domain (Indicated with "PB" in **Figure 7.1B**). The SA-1 peptide is a cyclic constrained peptide (i.e. it contains two cysteines that form a disulfide bond) that binds streptavidin directly (Bessette et al. 2004).

In single molecule experiments, it is advantageous to pre-form lower affinity bonds and/or bonds that are sterically difficult to reach, in bulk with high concentrations of ligands. In our experiment, the streptavidin-SA-1 bond is less strong than biotin-streptavidin and close to the bacterial cell surface, thus difficult to reach by a DNA-coated bead. Therefore, we pre-form this bond by incubation of cells with streptavidin, and in the single-molecule experiment, create a tether by allowing the biotinylated DNA on the bead bind to streptavidin that is bound on the bacterial surface.

The force-extension relation of a dsDNA molecule is well understood (Bustamante et al. 2000). At low forces, < 5 pN, the DNA molecule behaves like an entropic spring with a persistence length P~50 nm, and its force-extension behavior is well-described by the

inextensible Worm-like chain model (I-WLC). However, at higher forces (5-50 pN), the molecule can be extended beyond its contour length *L* (0.34 nm/bp), thus displaying an intrinsic elasticity where the chemical structure of DNA is altered. In this force range, a simple approximation has been reported in the literature, called the extensible Worm-like-chain model (E-WLC) (Odijk 1995), which gives good agreement with experimentally observed force-extension curves:

$$x = L(1 - \frac{1}{2}\left(\frac{k_b T}{FP}\right)^{1/2} + \frac{F}{S})$$ (**Equation 7.2**)

As the contour length *L* is known for our DNA molecule (2160 nm, see Materials & Methods), the model has two free parameters, the persistence length *P* and the stretch modulus *S*. These values depend on buffer and salt conditions; an overview of reported values is given in **Table I**. We chose a persistence length of 50 nm, and a stretch modulus of 1000 pN. Although it is possible to fit the expression to our experimental data and obtain *P* and *S* for our conditions (see Materials and Methods), the E-WLC model curve obtained with these parameters was good enough for our purposes and was used throughout this chapter.

In this chapter, we first calibrate the geometry in which the bacterial tethers are formed, using DNA tethers between an immobilized bead and a trapped bead. Then, we analyze force-extension curves of bacterial tethers. Comparison is made with the DNA

Persistence length	Stretch modulus (pN)	Salt concentration	Buffer conditions	Reference
47 nm	1008	10 mM Na+	Phosphate pH 7.0, 0.1 mM EDTA	(Wang et al. 1997)
43 nm	1205	150 mM Na+, 5 mM Mg2+	Phosphate pH 7.0, 0.1 mM EDTA	(Wang et al. 1997)
53 nm	NA (I-WLC)	10 mM Na+	Phosphate pH 7.0	(Smith et al. 1992)
51 nm	1087	150 mM Na+	Tris pH 8.0, 1 mM EDTA	(Smith et al. 1996)

Table I. Experimental values for the Persistence length and Stretch modulus of dsDNA. The persistence length values were obtained from fitting to the I-WLC model (forces < 5pN), whereas the stretch moduli were obtained from fitting to the E-WLC model (2 pN < forces < 50 pN).

tethers between beads and two different strains, which differ only in the presence or absence of an internal anchoring of the OmpA β-barrel to the peptidoglycan cell wall.

Results

DNA tethers to an immobilized bead

The experimental geometry employed is shown in **Figure 7.2A**. Biotin- (d = 3.28 μm) or streptavidin- (d = 6.7 μm, Spherotech) coated polystyrene (PS) beads were aspecifically adhered on the surface of a flow chamber (see Materials and Methods for details). Then DNA-coated PS beads (d=1.87 μm, Spherotech) were flushed in and the sample was transferred to the optical trap. A DNA coated bead was optically trapped, and after recording a power spectrum (giving the trap stiffness k_x and k_y), the bead was brought into close proximity to an immobilized bead by moving the stage. Then, the stage was moved away at a constant speed (either 2.4 μm/s or 0.24 μm/s, termed "fast" and "slow", respectively).

When a DNA tether has formed, the trapped bead will be pulled away from the trap center. The displacement of the bead from the trap center was determined from recorded video images (25 Hz) by a centroid cross-correlation method (Gelles et al. 1988), and converted into force assuming the linear relationship $F = kx$. Comparing DNA force-extension curves obtained at different trap stiffnesses, we estimate that displacements of the bead are linear with force up to ~300 nm (see **Figure 7.4B**). It follows that accurate force determination is possible up to a maximum of 30-60 pN depending on the trap stiffness (100-200 pN/μm). Care was taken to measure the trap stiffness 4-5 μm away from the surface.

If the trapped bead is displaced along the camera X- or Y-axis only, it is sufficient to take only the x or y-values of the tracked stage and trapped bead. We define the tether length as the length of the DNA molecule l_{DNA} plus the DNA-bead radius:

$$x_{tether}(t) = l_{DNA} + r_{bead} = x_{tether}(0) + x_{stage}(t) - x_{bead}(t)$$
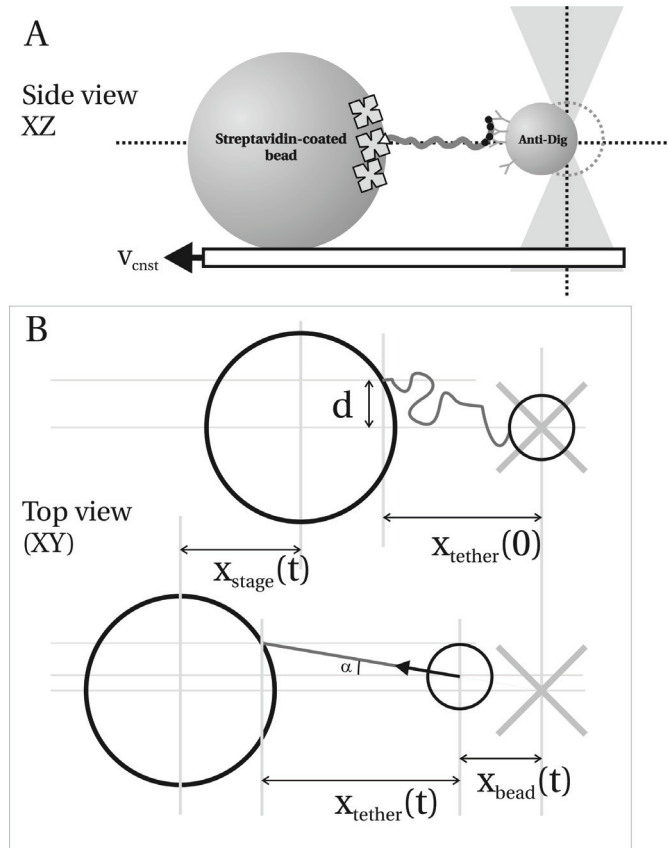
Figure 7.2: DNA force-extension (F-x) curves between an immobilized bead and a trapped bead. **(A)** Side view of the experimental geometry. **(B)** Analysis of the video data. The stage displacement in the pulling direction (here along the x-axis) is obtained from video tracking the position of the immobilized bead. The off-axis tethering distance d is indicated. The tether has an unknown length when the recording starts at t = 0 ($x_{tether}(0)$ in upper situation). After stage displacement over distance x_{stage}, the DNA molecule is extended, and force builds up. This force is obtained from video tracking the position of the trapped bead. Due to the force, the trapped bead is pulled out of the trap center by a distance x_{bead}, under an angle α. At forces > 5 pN, this angle can be approximated as a constant (see text). The DNA length is now given by $l_{DNA}=((x_{tether}(0)+x_{stage}-x_{bead})/\cos(\alpha))-r_{bead}$. We can choose $x_{tether}(0)$ such that the experimental F-x curve is super-imposed onto a theoretical F-x curve generated using the extensible Worm-like chain model (E-WLC).

However, if it displaces along both axes, a full analysis in XY is required (**Figure 7.2B**). Then, the force is given by the magnitude of the force vector

A
B
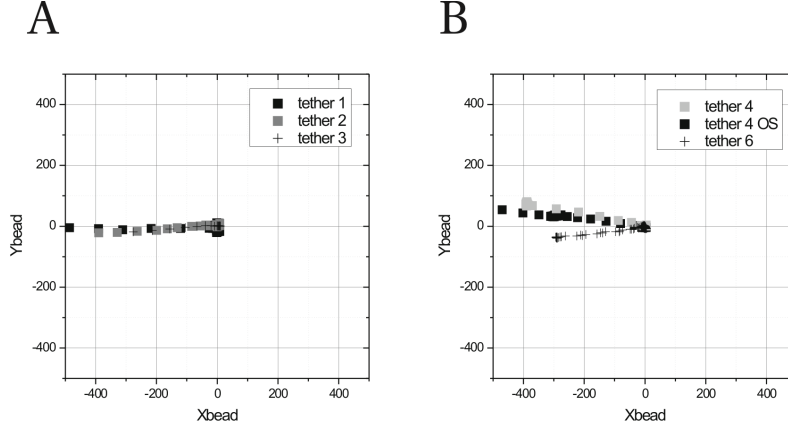
Figure 7.3: The position of the trapped bead determined by video tracking used to construct the DNA F-x curves shown in Figure 7.3. **(A)** Tethers obtained with immobilized biotin beads, **(B)** Tethers obtained with immobilized streptavidin beads. Although the type of bead does not matter for the shape of the force-extension curve, the distinction is kept here to for visual clarity of the graphs. Angles α were ~0° for tethers 1-3 (the left graph), ~11° for tether 4, ~7° for tether 4 OS (the difference is attributed to drift of the sample, as several minutes had passed between the first and the second curve) and ~7° for tether 6. All tracked bead positions for a given tether fall on a straight line. Therefore, as an approximation, the pulling angle α was taken to be constant during the force-extension curve.

$$F_r = \left| \vec{F}_r \right| = \sqrt{k_x x_{bead}^2 + k_y y_{bead}^2} = k_r \sqrt{x_{bead}^2 + y_{bead}^2} \; ,$$

with $k_x = k_y = k_r$ the lateral trap stiffness. The tether length must be changed in the length along the pulling angle α (defined as the angle of the force vector with either the (camera) X- or Y-axis) . For all force values in this chapter, the magnitude of the force vector was taken. For forces above ~5 pN, the DNA molecule is almost fully stretched (> 96% of the contour length) and the pulling angle is measured by α = *arctan(x_{bead}/y_{bead})*. There are two factors that introduce a non-zero value for the pulling angle α: (i) the pulling direction is not exactly aligned with the camera X-axis. This is a very small effect introducing an angle of ~0.8°. (ii) the tether attachment point on the immobilized bead can be off pulling-axis. For DNA tethers, this can be neglected also, as the maximum α we obtained was 11° (**Figure 7.3B**, tether 4). This underestimates the tether length with cos(11°): ~2%. For the bacterial tethers, however, a significant pulling angle up to 30-40°

(cos(40°) leads to ~25% under-estimation) was sometimes present (see below).

Note that in principle the pulling angle α is a function of the distance between the immobilized bead and the trap center (x_{stage}). If we define the off-axis tethering distance d (normal to the pulling direction), then the pulling angle follows from $\alpha = \arctan(d\,/(\,x_{stage} + x_{tether}(0)))$ (**Figure 7.2B**). However, in the region where we consider the pulling angle meaningful (i.e. when the forces are > 5 pN) the stiffness of the DNA molecule increases rapidly, causing small stage displacements to increase the force rapidly. Thus, for small Δx_{stage} we expect small $\Delta\alpha$.

This is shown experimentally in **Figure 7.3**, where the XY trajectories are plotted that trapped beads follow as the force on them increases. Tethers 1-3 were obtained on biotin beads, whereas tethers 4-7 were obtained on streptavidin beads. Indeed, the trajectories are approximately linear, with the pulling angles indicated. To get an impression of the experimental noise, we monitored the force angle for "Tether 4" at a constant DNA extension (force ~ 26 pN) and found that the angle fluctuated around 10.8±1.5°. So a meaningful accuracy here is ~1°. Therefore, for sufficiently stiff tethers, we can treat the pulling angle α constant, and we plot the force vector magnitude as a function of the extension along the x-axis (x_{stage} - x_{bead}) divided by $\cos(\alpha)$.

The resulting force-extension (F-x) curves are shown in **Figure 7.4A-C**. The F-x curve expected for a 2160 nm DNA molecule attached to bead of radius 935 nm (expected tether length when the DNA molecule is fully extended: 2160 + 935 = 3095 nm) given by the extensible worm-like chain model (E-WLC model: P=50 nm, S=1000 pN) is plotted for comparison. As the absolute length of the tether between the two beads is difficult to measure from the bright field images due to diffraction rings around the beads, the measured F-x curves were manually super-imposed on top of the E-WLC model (i.e. $x_{tether}(0)$ is used as fitting parameter). As can be seen in **Figure 7.4A-C**, all the F-x curves overlap with the E-WLC model and each other for forces below ~40 pN (provided the trap stiffness is sufficiently high, see **Figure 7.4B**). F-x curves obtained at both fast (2.4 μm/s) and slow (0.24 μm/s) pulling rates were found to overlap (**Figure 7.4C,** compare "Tether 4 slow" with "Tether 4 OS" below 40 pN). At forces above 40 pN, the well-known DNA over-stretching transition was observed. During over-stretching, the contour length of the molecule can be increased to ~170% with only little increase in force (Smith et al. 1996). This transition is interpreted as the melting of the two strands (Williams et al. 2001). In
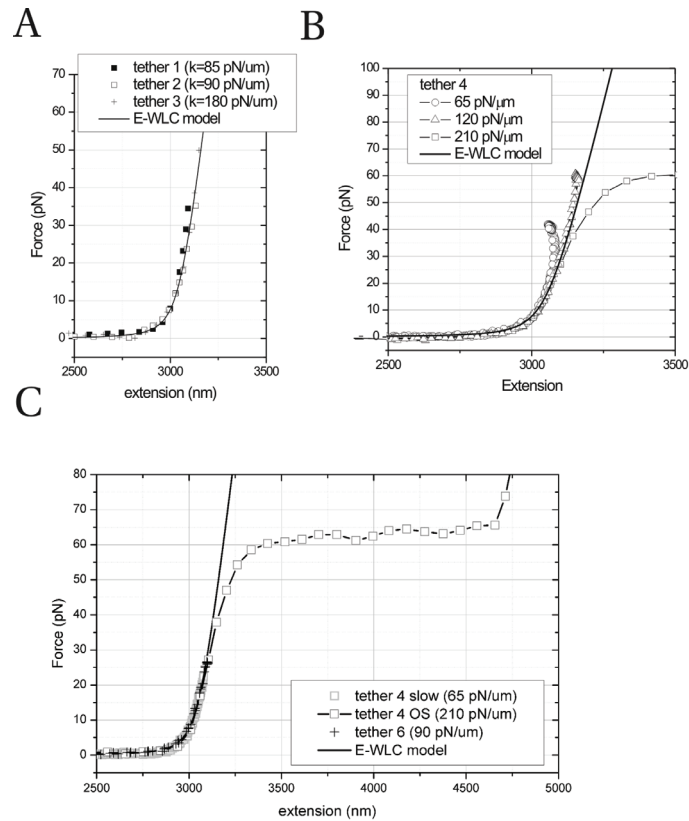
Figure 7.4. F-x curves of DNA tethered between an immobilized bead and a trapped bead. F-x curves of a 2.16 μm DNA molecule tethered between beads via biotin-streptavidin and digoxigenin-anti-digoxenin linkages. In all graphs, the black line curve is an extensible worm-like chain model (E-WLC) for a dsDNA molecule with a contour length of 2160 nm, a persistence length of 50 nm and stretch modulus 1000 pN, shifted with 935 nm to account for the bead radius. The experimental curves were shifted on the x-axis to super-impose them on the DNA model. Trap stiffness values are indicated. **(A)**: DNA tethers obtained with biotin beads (3.28 μm PS) and streptavidin-DNA-beads (where the biotinylated DNA was pre-incubated with streptavidin before mixing with anti-dig beads) **(B,C)**: DNA tethers obtained with streptavidin beads (6.7 μm, PS) and DNA beads. In **(B)**, the same DNA tether was extended at three different trap stiffness values. By comparing the obtained F-x curves we estimate that the linear regime for our bead/trap combination is ~300 nm (see text).

Figure 7.5B two more OS curves are shown. The overstretching plateau force was ~62 pN, and after extension to ~170-175% the force rapidly rises. The force plateau value is similar

to the value reported in literature (65 pN) (Smith et al. 1996).

To estimate the bead displacement range for which the trap is linear, the same DNA tether was extended at three different trap stiffness values (**Figure 7.4B**). We assume that for the highest trap stiffness k=210 pN/μm, the trap is linear up to 42 pN (200 nm). Then, we see that at around 40 pN, for k=120 pN/μm, the F-x curve starts to deviate from the expected F-x curve. The bead displacement is then ~300 nm. Furthermore, we see that at around 20 pN, for k=65 pN/μm, the F-x curve starts to deviate from the expected F-x curve. The bead displacement is then ~300 nm. This suggests that for a 1.87 μm PS bead in our setup, the trap is linear for bead displacements up to ~300 nm. Thus, our original assumption of a linear trap for k=210 pN/μm up to at least 200 nm is valid.

We conclude that the DNA tethers are very reproducible, and that a single E-WLC model can describe all experimentally obtained curves. In these experiments, both ends of the DNA molecule are in a plane roughly parallel to the surface of the flow-cell and through the center of the trapped bead when no force acts on it. As the bacterial tethers will have one end of the DNA molecule below this plane (typically 1-1.5 μm), we first study the effect of this on the F-x curves.

Axial dependence of the trap stiffness and trap center

When a bead is displaced in the axial (z-) direction (normal to the surface of the flow cell), its appearance changes (the diffraction rings change size etc.) After a DNA tether was formed, the immobilized bead was displaced along the axial direction to bring the two ends of the DNA molecule together in one plane normal to the z-axis. This was done in the following way: While continuously displacing the stage back and forward, pulling the tethered bead out of the trap center, the z-position of the immobilized bead was adjusted with the piezo-stage in 0.1 μm steps until visually, the trapped bead's appearance did not change when it was pulled on.

Then the stage was displaced either 0.5 or 1.0 μm down, increasing the distance between the trapped bead and the surface. Next, F-x curves were measured. From the recorded movies, we found that as the lateral force increases, the bead's axial position changes too, in the order of a few 100 nm (by comparing with images of a stuck bead displaced axially). Thus, we find that when one end of the DNA is tethered to a point 1 μm below the trap center, during an F-x curve, bead displacements in the lateral and the axial direction can be of the same order of magnitude! This can be understood if we realize that
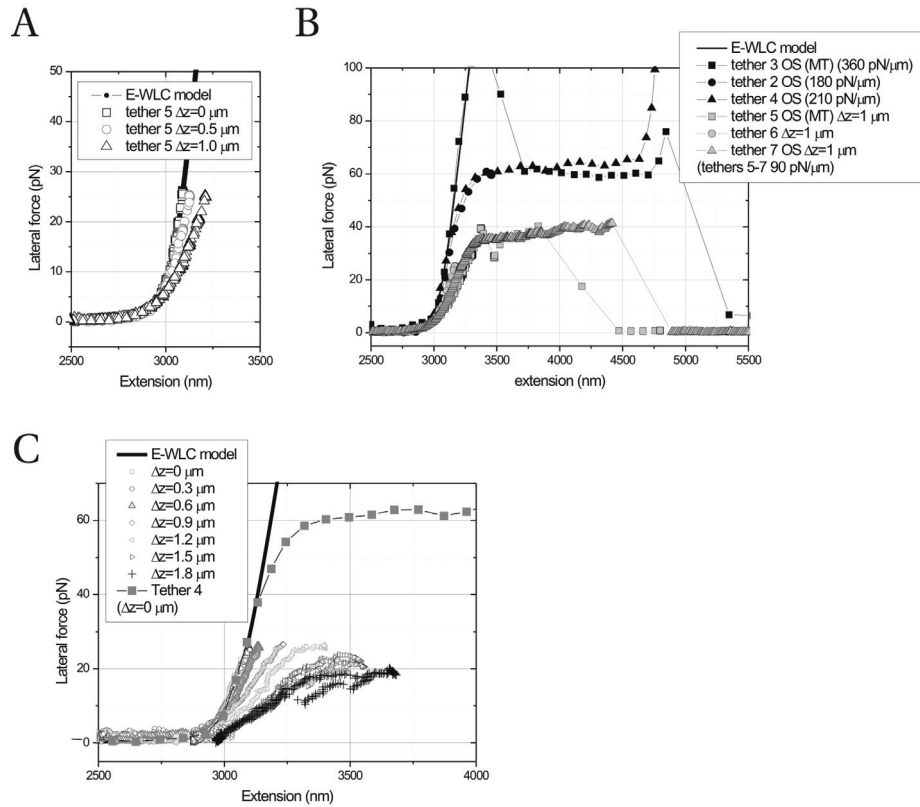
Figure 7.5. Influence of the axial z-position of the anchoring point on the F-x curves of DNA tethers between beads. Black line curve is the same E-WLC as in the previous figures. **(A)**: For Δz~0, the experimental curve super-imposes well on the theoretical curve. However, already at Δz=0.5 μm, for forces above a few pN the force increases less rapidly. This correlates visually with a change in axial position of the trapped bead. For Δz=1.0, the distance corresponding to that in the bacterial tethering experiment, these effects are further increased. **(B)**: Apparent lowering of the overstretching transition by a factor 1.5-2 due to axial displacement of the trapped bead during the F-x measurement. Black F-x curves are measured at Δz~0, gray curves at Δz~1.0 μm **(C)**: F-x curves obtained when increasing Δz in steps of 300 nm. Curves were shifted to super-impose on the E-WLC model at low forces. Curves were not corrected for pulling angle (for Δz=0, it was 11°). Note the presence of "thermal hysteresis" typically observed when over-stretching dsDNA for Δz=1.5 μm and 1.8 μm.

the axial trap stiffness is typically several times lower than the lateral trap stiffness (Wang et al. 1997; Rohrbach 2005).

In **Figure 7.5A**, F-x curves of a single tether (Tether 5) at $\Delta z=0$, 0.5 and 1.0 μm are shown. The curves were superimposed on the E-WLC model at low forces. As Δz increases, for higher forces, the slope increases progressively less fast than expected from the E-WLC model. This either indicates that the magnitude of the force is under-estimated for a given extension, or that the extension is over-estimated for a given force. As the extension is more likely to be under-estimated since for the extension the projection on the XY plane is used, most likely the force is under-estimated. In **Figure 7.5B**, several overstretching curves are plotted together, either at $\Delta z = 0$ μm (black curves) or at $\Delta z=1.0$ μm (gray curves). For the overstretching curves measured at $\Delta z = 0$ μm, as mentioned, the overstretching plateau occurred around 62 pN. Surprisingly, at $\Delta z = 1.0$ μm, the overstretching transition plateau force was reduced to ~35 pN! Apparently, the force is underestimated by almost a factor of 2 when the bead is laterally displaced over ~350 nm. Additional evidence comes from a series of F-x curves where Δz was varied in steps of 300 nm between 0 and 1.8 μm that exhibited a progressively reducing overstretching plateau down to 15-20 pN, complete with hysteresis that has been ascribed to re-annealing of locally melted DNA strands (Williams et al. 2001) (**Figure 7.5C**).

In an attempt to take into account the axial displacements, we used geometrical relations deduced in (Wang et al. 1997) to recalculate the force-extension curves for a given axial displacement $\Delta z=0$, 0.5 and 1.0 μm of the immobilized bead. Because we also take into account the pulling angle α, and use the magnitude of the force vector in XY, this makes the treatment fully three-dimensional. For a particular pulling angle α in the XY plane, after defining the R-axis as $R = X / \cos(\alpha)$, we can draw the corresponding RZ plane (shown in **Figure 7.6A**). If we assume that the lateral trap stiffness k_r is not a function of z then force balance dictates

$$\frac{F_r}{F_z} = \frac{k_r r_{bead}}{k_z z_{bead}} = \frac{r_{tether}}{z_{tether}} \quad (\textbf{Equation 7.3})$$

Here, $r_{tether} = x_{tether} / \cos\alpha$, and $z_{tether}=\Delta z - z_{bead}$. As Δz, r_{tether} and r_{bead} are known, we can solve for z_{bead}:

$$z_{bead} = \frac{\Delta z}{\left(k_z / k_r\right)\left(r_{tether} / r_{bead}\right) + 1} \quad (\textbf{Equation 7.4})$$

Choosing a value of 2.5 for the ratio k_x/k_z, a tether length of 3000 nm, a lateral trap stiffness of 100 pN/μm and Δz=1.0 μm, we find that when the force is 25 pN (r_{bead} is then 250 nm), z_{bead} is 172 nm. This confirms that for our experimental geometry, displacements in x and z can be of similar magnitude.

Now we recalculate the tether extension and force, using straightforward geometrical formulas given in (Wang et al. 1997), which can be obtained from the schematic diagram in **Figure 7.6A**:

$$\theta = \arctan\left(z_{tether} \Big/ r_{tether} \right), \; l_{DNA} = \frac{z_{tether}}{\sin\theta} - r \;, \; F = \frac{k_r r_{bead}}{\cos\theta} \quad \textbf{(Equation 7.5,7.6,7.7)}$$

As can be observed in **Figure 7.6B**, this correction brings the F-x data more in agreement with the expected E-WLC model, but not fully. However, in the Wang study, a feedback system was employed that increased the trap stiffness as the bead was pulled out of the trap. Their displacements were smaller than ours, and their assumption of constant lateral trap stiffness might not hold in our case. It has been shown that the lateral trap stiffness is a function of axial position (C. Tischer, unpublished), and is highest in the beam focus. As the trapped bead is pulled towards this focus in our experiment, it is therefore expected that the trap stiffness increases. If we try to recover the E-WLC model, we can get a reasonable agreement if we assume that $k_r(z)$ increases linearly with bead height, such that $k_r(300\,nm)=2k_r(0)$. The calculated force then becomes the apparent force and the real force is given by

$$F_{real} = (k_r + \frac{z_{bead}}{300}k_r)\frac{r_{bead}}{\cos\theta} = (1 + \frac{z_{bead}}{300})F_{app}$$

This can also explain the lowered overstretching plateaus at $\Delta z > 0$. The same 3D model was applied to the overstretching tether 7 that displayed an overstretching plateau force of ~35 pN (**Figure 7.5B**). After correction with the same $k_x(z)$ dependence, a F-x curve with the expected plateau force of ~65 pN is obtained (**Figure 7.6C**). This provides further evidence for an axial dependence of k_x on z, with a doubling of the lateral trap stiffness over a few hundred nm. This appears reasonable, as such distances are also in the order of what is usually reported for the axial bead position relative to the beam focus due to scattering forces. Since Δz is not exactly known for the bacterial tethers (axial positioning of the trap was performed manually in these experiments), in the following, we treat the tethers only in XY, but compare the resulting F-x curves to the F-x curves of "pure DNA"
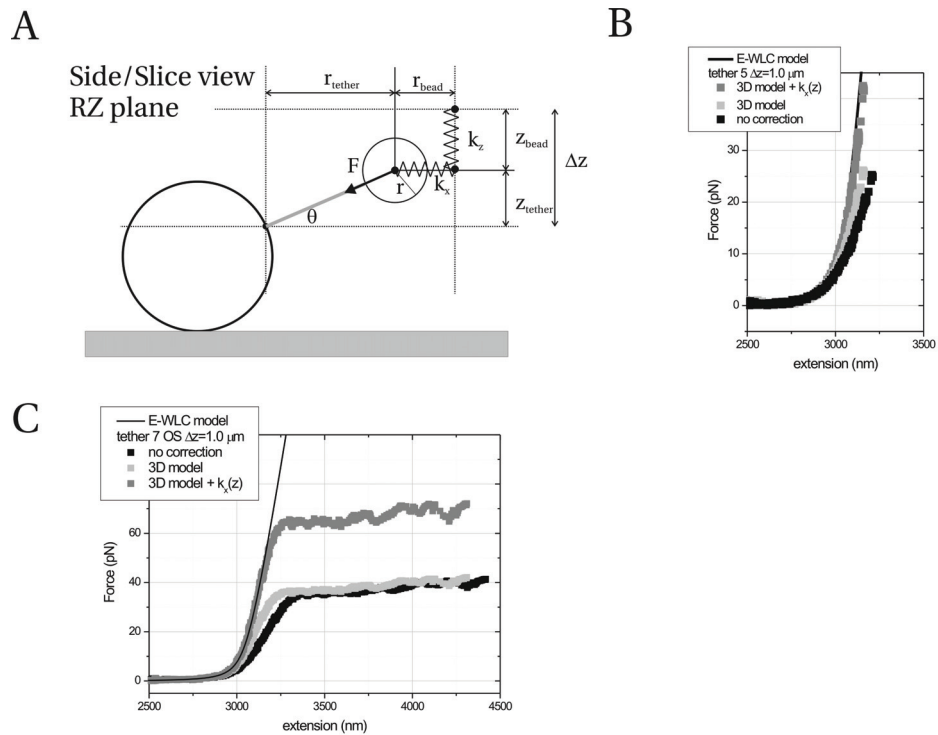
Figure 7.6: Correcting for axial bead displacement. (A): 3D geometrical model used to correct fo axial bead displacement (Schematic diagram of the RZ plane). From **Figure 7.2**, it follows that $r_{tether} = x_{tether}/\cos(\alpha)$, and $r_{bead} = \sqrt{x_{bead}^2 + y_{bead}^2}$. We assume that $k_z = k_x/2.5$. r is the bead radius (935 nm). Using the formulas discussed in the text, we calculate z_{bead} and θ, and subsequently F and the true tether length l_{DNA}. **(B)**: Graph that corrects tether 5 at $\Delta z = 1.0$ μm using the geometrical 3D model. After applying the correction, the match with the expected E-WLC model improves, but there is still a large discrepancy. If we assume that k_x and k_y are a function of the bead's axial position, and (arbitrarily) let them increase linearly from k to 2k over an axial distance of 300 nm, we obtain a curve that can be super-imposed on the E-WLC model. **(C):** the same 3D model applied to the DNA overstretching curve of tether 7 (**Figure 7.5**). The overstretching plateau now lies at ~65 pN, the expected value.

tethers for different Δz values.
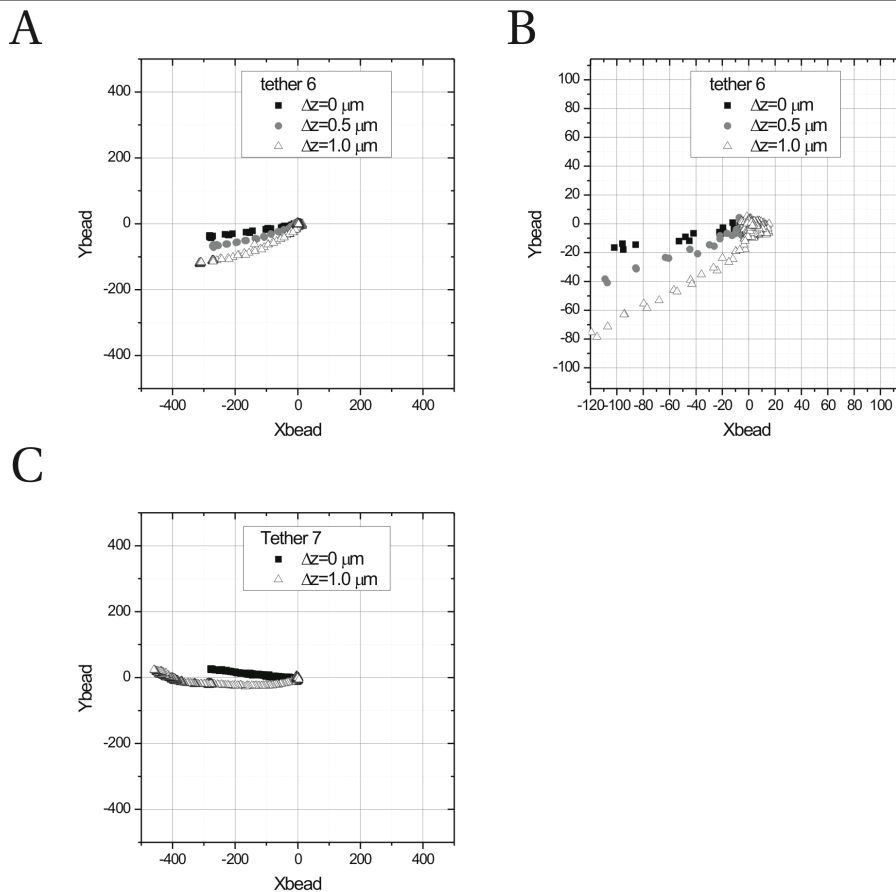
Figure 7.7. The position of the trapped bead determined by video tracking during F-x curves at different Δz. When Δz is non-zero, the bead positions at high forces no longer follow a straight line but a continuously curved trajectory. At low forces, the pulling angle is a function of Δz. **(A):** Tether 6 (a single tether) at three different heights (Δz=0 μm, Δz=0.5 μm and Δz=1.0 μm). **(B):** Zoom-in on tether 6: the pulling angle α in the low-force regime changes with Δz: from ~10° to ~21° to ~34°. **(C):** Tether 7 OS.

Surprisingly, for $\Delta z > 0$ μm, not only the force-increase is reduced, also the bead's XY trajectory no longer is on a straight line, but on a curved trajectory. This is visible from an XY plot of the trapped bead for tether 6 and tether 7 (**Figure 7.7A and 7.7C**) (the F-x curves for tether 6 and 7 were plotted in **Figure 7.5B**). All tethers at non-zero Δz showed increased curving with Δz.

Because the bead appearance changes when it is axially displaced, and the video-

tracking algorithm uses a single reference image of the bead for all frames, we checked whether this could lead to artifacts in detected bead position. Manually, for each subsequent frame, the bead image from the previous frame was used to find the change in bead position. Summing these relative bead changes then yields the position of the bead for each frame. Comparing these with the automated procedure based on a single reference images, similar (curved) XY bead trajectories were found, thus excluding a video-tracking artifact.

At forces > 5 pN, the curves are approximately linear again, as observed before. However, as can be seen in the zoom-in (**Figure 7.7B**), the pulling angle α is now a function of Δz, as if the anchoring point off-axis (coordinate *d*) changes with Δz. However, we verified that the center of the immobilized bead only changes a few tens of nm when the stage is displaced over 1 μm in the axial direction. This is expected to have a negligible effect on the pulling angle. We can also exclude drift of the immobilized bead with respect to the trapped bead as the cause, since from video tracking this was found to be ~1 nm/s and the experiment was performed within ~30 s. Furthermore, the trapped bead's XY trajectories were reversible upon reducing Δz again.

Possibly, the trap center (i.e. zero force position of the trapped bead) changes along the optical axis, due to imperfect alignment of the laser beam or asymmetries in the trap focus. More experiments are needed to test this hypothesis. For example, using the XYZ telescope that controls the position of the laser focus inside the specimen, a trapped particle can be moved through the image plane to visualize the optical axis.

Bacterial tethers to the OmpA β-barrel

A side view of the bacterial tether assay is drawn schematically in **Figure 7.8A**. The bacterium (pre-incubated with streptavidin) is stuck on the surface of the cover slip, and a DNA bead is pressed on top of the bacterium to form a biotin-streptavidin bond between the DNA molecule and the cell, after which the stage is moved away.

How to firmly attach a bacterium to a cover slip? We found that the positively charged biopolymer poly-L-lysine commonly used to immobilize bacteria was not compatible with negatively charged DNA-coated beads. Previously, DNA tethers to bacteria have been used to study DNA import in competent *B. subtilis* ((Maier et al. 2004; Hahn et al. 2005), In these studies, the bacteria were immobilized to silanized cover slips. However, the authors reported slippage events at forces > 4 pN and bacteria detaching from the surface. We tried
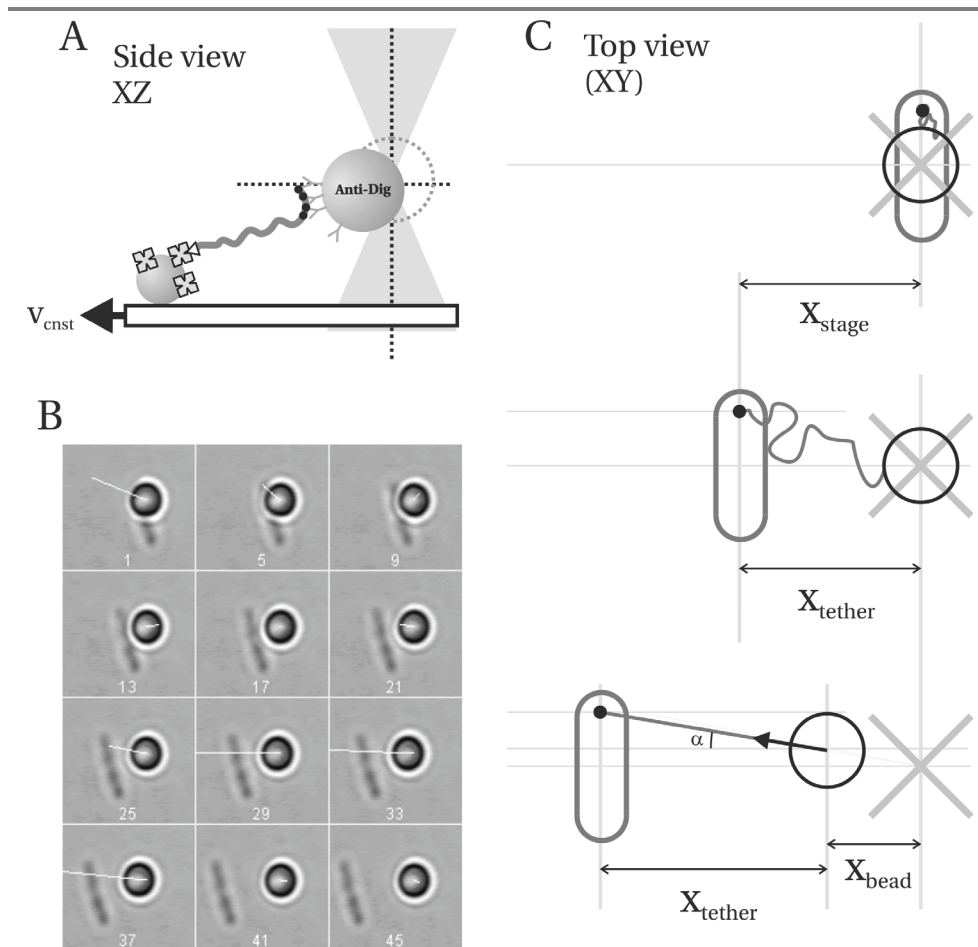
a 2% solution of dimethyldichlorosilane dissolved in octamethyl cyclo-octasilane (Amersham Repel-silane), but bacterial sticking did not increase compared to untreated glass. In the end, we chose a procedure in which chromic-sulfuric

acid is used to etch away a layer of glass to create a clean glass surface. We found that when the slides were stored immersed in milliQ, over a few weeks, the adhesion properties of the slides would decrease, and a new batch was prepared.

First, we discuss results from a strain that expresses the OmpA β-barrel that should be free to move in the outer membrane (see also the discussion in **Chapter 8**). From the ~120 tether attempts, in most cases the bacterium was pulled off the surface by the trapped

Figure 7.8. Bacterial tethers. **(A) The experimental geometry.** The bacterium (pre-incubated with streptavidin) is adhered aspecifically to a glass surface. A tether is formed by positioning the trapped DNA-coated bead above the bacterium, bringing them into contact for ~15-20 s to form a biotin-streptavidin bond, and after increasing the axial distance of the trapped bead again, displacing the stage either in X- or Y-direction, depending on the orientation of the bacterium. **(B) Image sequence of a bacterial tether (Tether 5 in Figs. 7.9 and 7.11) that breaks between frames 37-41**. Frame numbers are shown; the movie is recorded at 25 fps. Plotted in each frame is the force vector, calculated from video tracking data of the trapped bead. The length of the vector was made to scale linearly with the magnitude of the force. **(C) Analysis of bacterial force-extension curves.** The calculation of the force-extension data is done in the same way as for DNA tethers between beads, except that now, the stage position and bead center overlap when recording starts. For the analysis, this does not matter. For the last step, super-imposing the F-x curves on the E-WLC model by shifting along the extension axis, this is still allowed, but only to an extent of the diameter of the bacterium, i.e. ~1 μm. This is based on the idea that the pulling angle α provides the anchoring point on the bacterium along its long axis, but that tethering can occur anywhere along the short axis.

bead, sometimes with the bead stuck directly to the bacterium, but also many times clearly via a DNA tether (dragging the bacterium over the surface). In 20 cases, this resulted in tether formation while at the same time the bacterium remained stuck on the surface. A typical tethering event is shown in **Figure 7.8B** (*E. coli* OmpA-177 tether 5). The time between subsequent images in **Figure 7.8B** is 160 ms (not all frames are shown). Plotted also is the force vector on the trapped bead, with the length of the white line proportional with the force.

It was found that ~30 min after addition of the DNA beads to the flow-cell, hardly any tethers could be formed anymore. The thermal off-rate of the SA-1 peptide is $10^{-3} \, s^{-1}$, which means that the average bond lifetime is 17 min. We suspect that streptavidin unbinding from cells in the sample, followed by rebinding onto the biotinylated ends of the DNA causes the observed decrease in tether formation. Due to the high affinity of the biotin-streptavidin interaction and the low amount of biotinylated DNA present on the beads, very low streptavidin background concentrations could already block all tether ends. To circumvent this problem, every 30 minutes, a new dose of DNA beads was flown through the sample. This also prevented the (open) flow-cell from evaporating.

For all 20 tethers, we measured the tether length (r_{stage}-r_{bead}) when the force had reached 15 pN. From the E-WLC model of our DNA molecule, shifted with 935 nm to account for the bead radius, at 15 pN a tether length of 3048 nm is expected. We found an
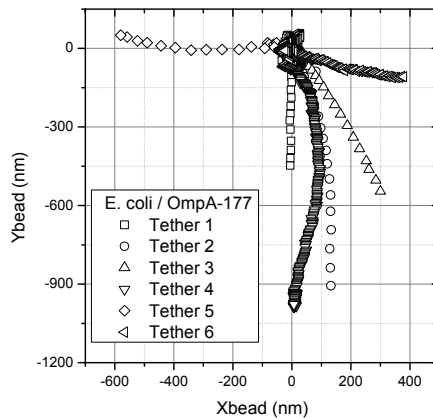
Figure 7.9: The position of the trapped bead determined by video tracking used to construct F-x curves of bacterial tethers to the OmpA-177[SA-1] β-barrel protein (shown in **Figure 7.11**). Tethers 2-5 show (at high forces) the continuous curving observed previously for "pure" DNA tethers at a Δz~1 μm. Possibly, along two orthogonal axes the curving is absent, however, experiments that systematically vary the pulling angle are needed to clarify the origin of the curving. For a tilted optical axis, only one symmetry axis is expected.

average bacterial tether length of 2837 ± 895 nm (S.D.). Because we under-estimate the tether length (by taking the projection on the XY plane, and ignoring a possible pulling angle α), this indicates that below 15 pN, the bacterial DNA tethers have lengths that are similar to DNA tethers between beads. The large spread is not surprising, since the tether will not be formed *exactly* underneath the trap center, but more likely somewhere on the bacterium within a radius of several hundred nm from the trap center.

For several tethers, a slight reorientation/"jump" (~100-300 nm) of the bacterium was visible after the tether broke. This indicates that the bacterium was not completely immobilized and acted as an additional spring as the force increased. Note that it is unlikely that the bacterium actually bends, since higher forces are expected to deform the shape-determining PG cell wall over several hundred nm (F >0.5 nN) (Boulbitch 2000; Boulbitch et al. 2000). Instead, compliances in the adhesion sites are likely to be present.

After restricting ourselves to tethers where (i) no sign of multiple tethers was present (i.e. multiple peaks in the F-x curve, and single-step breakage to zero), (ii) the angle between the long axis of the bacterium and the direction of stage displacement (either X-
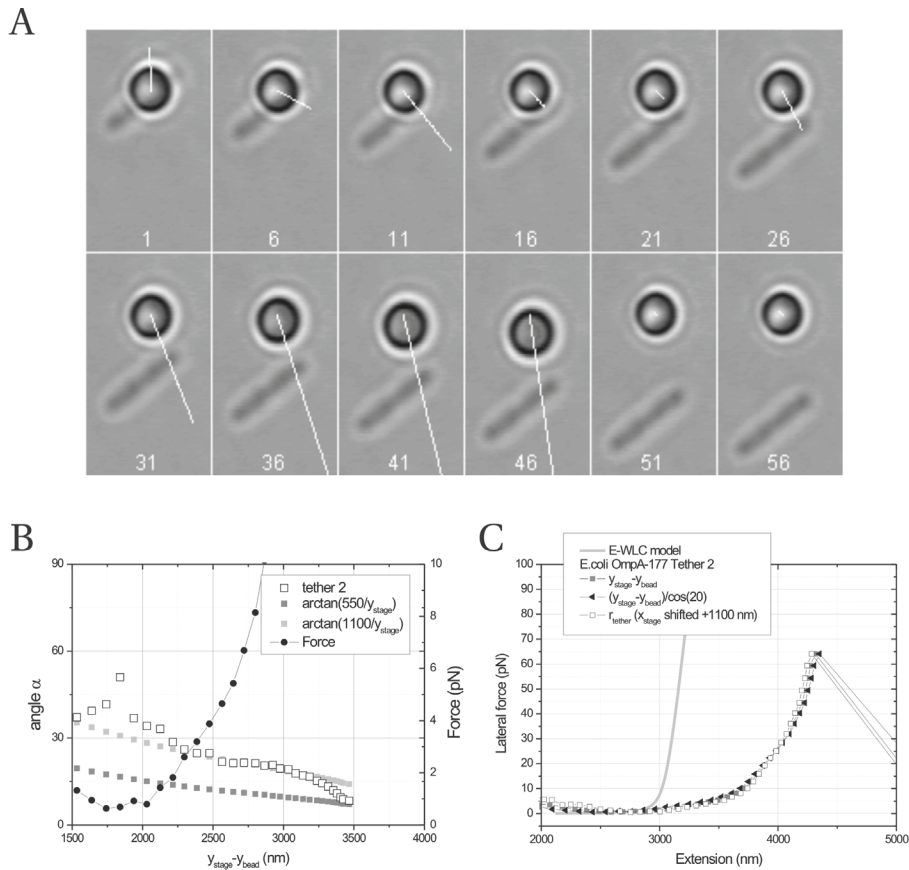
Figure 7.10. Determining the "true" tether extension. (A) Tether 2 image sequence. The force vector is displayed as a white line. Frame numbers are indicated. Movie was recorded at 25 fps. **(B)** The pulling angle α as a function of tether extension, obtained from the force-angle of Tether 2 (see also **Figure 7.9**), compared with two arctan() functions expected for either 550 nm or 1100 nm off-axis anchoring. **(C)** Comparison of three ways to calculate the tether extension (see text), all shifted to overlap the E-WLC model at low force (~1 pN). All corrections are minor compared to the overall shape of the curve.

or Y- direction) was greater than 45 degrees (to minimize the risk of creation of additional specific or aspecific tethers as the bead moves over the bacterium) and (iii) no visible displacement of the bacterium was present, 7 tethers remained. Of these seven, one was dropped, as the force vector did not point to the bacterium but to a point on the cover slip, suggesting that it was a surface tether. Note that condition (iii) implies that the bacterium

displaces less than a pixel (say < ~50 nm) over a force range of ~50 pN, and therefore can be considered a (stiff) spring with stiffness > ~1000 pN/μm.

For all bacterial tethers, the visual appearance of the bead indicated that it displaced axially as well as laterally. This is expected, as the attachment point on the bacterium is ~one bead radius below the trap center. Again, we plot the tracked XY positions of the trapped bead during a F-x curve, shown in **Figure 7.9**. If we restrict ourselves to the linear regime of the trap (~300 nm, see **Figure 7.4B**), the trajectories of tethers 1,3,5 and 6 are approximately linear. Tethers 2 and 4 show a curved trajectory already below 300 nm.

A selection of frames for Tether 2 is shown in **Figure 7.10A**, with the force vector indicated by a white line. The force angle of tether 2 is plotted as a function of extension (here simply taken as y_{stage}-y_{bead}) in **Figure 7.10B**. Possibly, at low forces, the DNA is entropically coiled-up, undergoes a drag force exerted by the fluid and the force vector does not point necessarily in the right direction. When the DNA is straightened out (at forces >3 pN), the force angle is well-described by the $\arctan(d / y_{stage})$ function, assuming an anchoring point d 1100 nm off-axis. Around 2750 nm, the force starts to increase rapidly. It is in this regime that we approximate the pulling angle as a constant (here ~20°). Furthermore, for forces above 30 pN (Above 3250 nm "extension"), the pulling angle starts to deviate from the $\arctan()$.

This could indicate that the anchoring point on the bacterium changes. Note that if it does, it does so in the "wrong" direction (i.e. in the direction opposite to the direction that is expected to decrease the tether length and therefore the force). However, as the bead is no longer in the linear regime, and similar changes in pulling angle have been observed for "pure" DNA tethers anchoring below the trap center, it is as well possible that the trap center changes. For now, we are careful with extrapolating the force vector to make statements about possible relocation of the anchoring point.

What is the proper level of accuracy when analyzing bacterial tethers?

Next, we evaluate three progressively more refined ways to plot the F-x curve for a tether that is anchored "off-axis" at a distance d normal to the axis defined by the pulling direction and the trap center, such as tether 2. The first is the "coarse" approach, by ignoring tether length under-estimations due to the pulling angle, and just plotting $y_{tether}=y_{stage}$-y_{bead}, as a function of the magnitude of the force vector F. A difference with the

F-x curves for DNA in between beads is that here, at *t=0*, the stage position y_{stage} (approximately) coincides with the bead position y_{bead}. Thus, the tether length is now given directly by y_{stage}-y_{bead}. Shifting the F-x curve on the x-axis to superimpose on the E-WLC model is now only allowed over a maximum of ~$\pi/4$*d/cos(α) (uncertainty on the bacterium) + (l_{DNA} + r)(1 – cos(α)). (Here, α=~20° so maximum shift is ~1000 nm, and a bit more since we also underestimate the length due to XY projection) to account for the uncertainty in where on the bacterium the tether is attached. The F-x curve in **Figure 7.10C** was shifted +850 nm to overlap at ~1 pN with the E-WLC model.

The second is the approach already used for the DNA tethers: from the bead XY displacements, a pulling angle α is estimated, and the tether length is increased by dividing with cos(α). For tether 2, this angle was ~20° (see above). Now only a +500 nm shift is needed to overlap the E-WLC model at ~1 pN, because all tether lengths are increased to 111% (**Figure 7.10C**).

Alternatively, an off-axis tethering point can be estimated (e.g. the d = 1100 nm off-axis above), and the length vector between this point and the bead center is used as the tether extension. This was done by shifting the *(x_{stage}, y_{stage})* coordinates with (+1100,+0). The pulling angle is now no longer a constant, but a function of *(x_{stage}, y_{stage})*. This approach ignores the actual force angle, and therefore ignores possible relocations of the anchoring point. This correction needed a +700 nm shift.

When we compare the three corrections, we find that all corrections are minor effects, and that compared to the spread in the different F-x curves (see below), it suffices to use a "coarse" approach, based on the most simple tether length, i.e. either x_{stage}-x_{bead} or y_{stage}-y_{bead} (depending on the pulling axis).

Bacterial F-x curves

Using the "coarse" approach, the force-extension curves for the 6 tethers are plotted in **Figure 7.11**. For comparison, the (over-stretching) F-x curve of "pure" DNA tether 7 (Δz = 1 μm) is reproduced from **Figure 7.5**. In **Figure 7.11A**, the F-x curves are plotted up to the end of the linear trap regime (x_{bead}~300 nm). From the 6 tethers, (for forces > 5 pN) tethers 5 and 6 appear similar to the "pure" DNA tether, whereas tethers 1-4 appear softer (less stiff). In **Figure 7.11B**, the full F-x curves are plotted. For tether 4 and tether 5, overstretching is observed, although the trapped bead is way outside the linear regime of the trap in both cases (x_{bead} ~600 nm for tether 5, and x_{bead} ~1000 nm for tether 6).
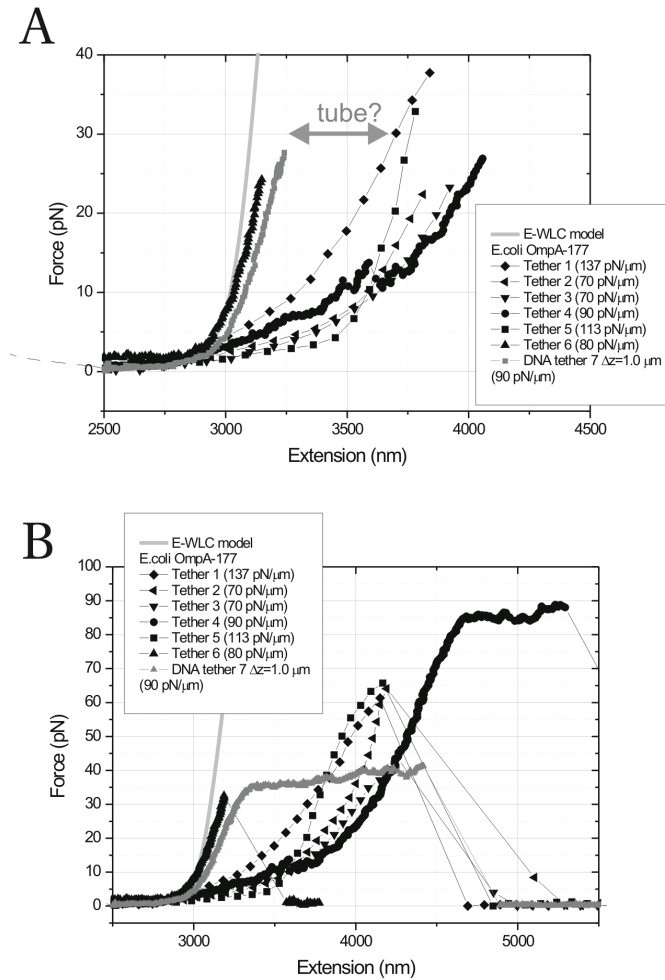
Figure 7.11. Tethers from strain MC1061 expressing OmpA-177[SA-1]. The force on the bead is plotted as a function of tether extension. For comparison with DNA tethers, both the E-WLC model and DNA tether 6 at $\Delta z=1.0$ μm are reproduced. The trap stiffness values for each curve are indicated. **(A)** As the trap is no longer harmonic for bead displacements $x_{bead} > \sim 300$ nm, we truncated the curves at this point to allow quantitative comparison between the curves. **(B)** The complete curves for the data shown in **(A)**.

Therefore, the actual OS plateau forces are (much) lower. Possibly, also for tether 1 the onset of overstretching is apparent at high forces.

As the bacterial tethers were created manually by repositioning the sample in the *z*-axis, it is possible that the softer tethers are "pure" DNA tethers at increased relative height between bead and bacterium ("Δz"). As the height increases, the slope of the F-x curve goes down (**Figure 7.5C**). Alternatively, additional compliance is present. As estimated earlier, for these selected tethers, the immobilized bacterium acts as a stiff spring > 1000 pN/μm. A tether length increase of > 50 nm relative to a "pure" DNA tether is therefore most easily explained by the formation of a membrane tube pulled from the bacterial outer membrane. For example, tether 1 at 30 pN could consist of a DNA tether 1 μm above the bacterium attached to a membrane tube of ~400 nm (estimated as the additional extension relative to the "pure" DNA tether at Δz = 1.0 μm). An alternative explanation would be that no tube is formed and the OM as a whole is displaced, i.e. the distance between PG cell wall and OM is increased without formation of a tube. However, based on our current understanding of the composition of the cell envelope of *Escherichia coli*, a large-scale displacement of the outer membrane away from the PG cell wall over distances more than a few nm would require the rupture of tens to hundreds of molecular bonds, which is unlikely.

What is puzzling for the "softer" tethers (tethers 1-4) is the absence of DNA OS at forces similar to that of the "pure" DNA tether (~35 pN). For the bacterial tethers, trap stiffnesses are 70-134 pN/μm, similar to the trap stiffness for which the "pure" DNA tether was obtained (90 pN/μm). For the Δz argument, tethers softer than "pure" DNA must be obtained at increased Δz (> 1.0 μm). For tethers 1 and 4 (trap stiffnesses 90 and 134 pN/μm), one then expects an OS plateau force below ~35 pN. However, the observed (onset of) overstretching for these tethers is at ~70 and ~85 pN, respectively. This argues against Δz being larger than 1.0 μm. Although we cannot rule out that both tethers consist of multiple DNA tethers that break in a single step, we consider this unlikely.

Thus, we must assume that tethers 1 and 4 were obtained at a decreased Δz (< 1.0 μm). Then tube-formation is required to explain the observed "softer" F-x curves. As tethers 2 and 3 are only linear up to ~21 pN, possibly the force does not become high enough to observe OS. For these tethers we cannot distinguish between Δz and tube.

Next to the 20 bacterial DNA tethers discussed above, 2 additional tethers (referred to as OmpA-177 tether 7 and 8) were obtained with extension lengths much longer (6-7 μm) than the DNA contour length (2.16 μm). See **Figure 7.12B**. Tether 7 starts with a DNA
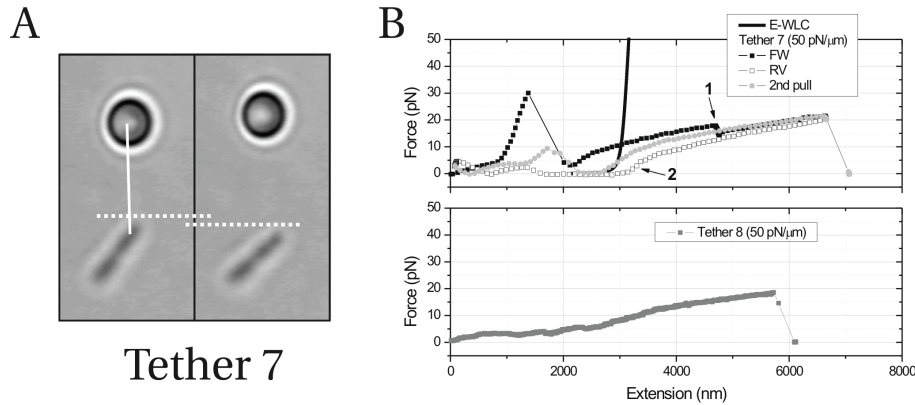
Figure 7.12. Possible membrane tubes pulled from strain MC1061 expressing OmpA-177[SA-1]. (A) Two frames from a movie in which a bacterial tether is formed that is much longer than the DNA contour length. After the tether breaks, the bacterium "snaps" back ~ 400 nm. The presence of a long tether is indicated by a white line. **(B)** Force-extension curves of bacterial tethers that were much longer (length 6-7 μm) than the majority of bacterial tethers (length 3 μm). Tether 7 was obtained at the "fast" pulling rate, tether 8 at the "slow" pulling rate. For Tether 7, arrow "1" indicates the moment where the stage was halted for 10 s during which the bacterium rotates over ~100 nm towards the bead, thus reducing the force. Comparing the forward and reverse curves of the first pull of tether 7, the anchoring point has reoriented over ~1000 nm (suggested from the shape near arrow 2), assuming a purely elastic response.

tether as inferred from the rapid force increase around 1000 nm. After this tether breaks, a second tether gradually pulls the end of the bacterium in the direction of the bead. When the force has reached ~17 pN, the stage was halted for 10 s (arrow 1 in **Figure 7.12B**). During this time, the bacterium further reorients ~100 nm, causing the force to decrease (stage drift was ~ 1 nm/s). However, when stage displacement continues, the tether is extended a further 3000-4000 nm up to a final extension up to 7 μm, after which the stage motion was reversed. A second pull resulted in a similarly shaped F-x curve above 2600 nm, shifted +400 nm. This shift is interpreted as a reorientation of the bacterium. During the F-x curve, the force increase / nm extension (slope of the curve) was remarkably low. At forces > 10 pN (with the bacterium under tension), the tethers displayed approximately linear force-extension behavior with an effective spring constant of ~3 pN/μm. Tether 8 has a similar F-x curve, extends up to 6 μm before it breaks, and has a similar effective spring constant.

Recently, a paper (Jauffred et al. 2007) described membrane tethers extracted from *E. coli* by optical tweezers. The tethers were formed directly between an (aspecifically adhered) PS bead and the bacterium. The tethers described by the authors had lengths several times the bacterial length (up to tens of microns long), a linear F-x curve through the origin, and a spring constant of 10-12 pN/μm for first-pull tethers, which was reduced in subsequent pulls.

Based on tether length and the soft linear F-x behavior, it is likely that our long tethers are in fact membrane tubes. Because for tether 7, only around ~3000 nm the bacterium reorients and force builds up in the tether, it is likely that the tether consists of a DNA molecule attached to a membrane tube. As in tether 8, a clear sign of a DNA molecule is missing, it is possible that this tether is a tube that was pulled through a direct bead-cell attachment.

Interestingly, upon reversal of the stage motion, the F-x curve has the same shape. In Jauffred *et al.*, after formation of a membrane tube at speeds similar to our "slow" speed, a viscous relaxation with a relaxation time of ~200 s to a lower "equilibrium" force plateau was observed. Here, however, both "fast" (tether 7) and "slow" (tether 8) pulling rates result in similar F-x curves. This suggests that during tether formation in our system, no viscous contribution is present. However, these data do not exclude that after (elastic) formation, an additional process (one that does not play a role during tether formation) might cause a viscous relaxation in these tethers.

To summarize, although we cannot rule out that the "soft" tethers are simply DNA tethers at increased heights above the bacterium, the fact that no overstretching at forces <35 pN is observed for these tethers despite their single-step breakage, and the fact that 2 of 22 tethers showed characteristics of extended OM membrane tubes, suggests that the "soft" tethers consist of a membrane tube in series with a DNA tether.

Bacterial tethers to full-length OmpA

As wild-type OmpA has a C-terminal periplasmic domain that anchors it to the cell wall, we also pulled tethers on a strain expressing such a construct (see also **Chapter 3**, and **Figure 7.1B**). From the ~150 tether attempts, 22 resulted in tether formation while at the same time the bacterium remained stuck on the surface.

Again, for all 22 tethers, we measured the tether length (r_{stage}-r_{bead}) when the force had reached 15 pN. We found an average bacterial tether length of 2712 ± 665 nm (S.D.).
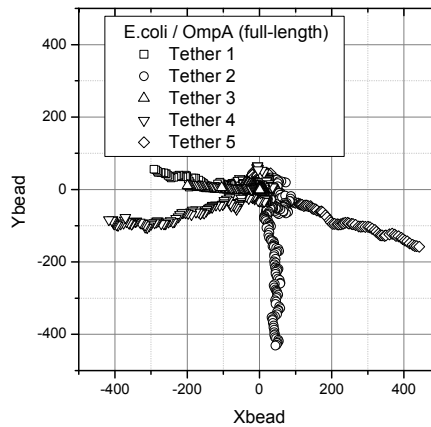
Figure 7.13: The position of the trapped bead determined by video tracking used to construct DNA force-extension curves of bacterial tethers to the full-length OmpA (shown in **Figure 7.14**).

Compared to the average tether length of 2837 ± 895 nm (S.D.) measured for the OmpA-177 β-barrel, this is ~100 nm shorter. Thus, both values are similar.

After setting the same constraints as for OmpA-177, 5 tethers remained. Again, we choose the "coarse approach" to plot the F-x curves, with only the x- or y- displacements used to calculate the tether extension. The XY scatter plots of the trapped bead are shown in **Figure 7.13**. The resulting F-x curves for these five tethers are plotted in **Figure 7.14A,B**. For comparison, a F-x curve of "pure" DNA Tether 7 at Δz=1 μm is reproduced from **Figure 7.5**.

Applying the same rationale as with the truncated OmpA tethers, we reason as follows: Tethers 4 and 5 are as stiff as a "pure" DNA tether at Δz = 1 μm. Tethers 1-3 are less stiff. Examining the tethers for the presence of an OS plateau, we find that tethers 1-4 show (the onset of) OS at forces varying from 20 pN (tether 3) to 35 pN (tether 1 and 4, for tether 4 over-estimated due to beyond linear regime) to 45 pN (tether 2, over-estimated as well). For tether 5, no OS is observed: for this tether the OS plateau is at least > 40 pN (end of linear regime). Thus, tethers 1-4 suggest "stiff" DNA tethers at around 1 μm height above the bacterium. Tether 5 completely overlaps with a "pure" DNA tether at 1.0 μm height, except that it does not exhibit a reduced OS plateau. There are two explanations possible for a higher OS plateau: either Δz < 1 μm or a multiple tether that shows single-step
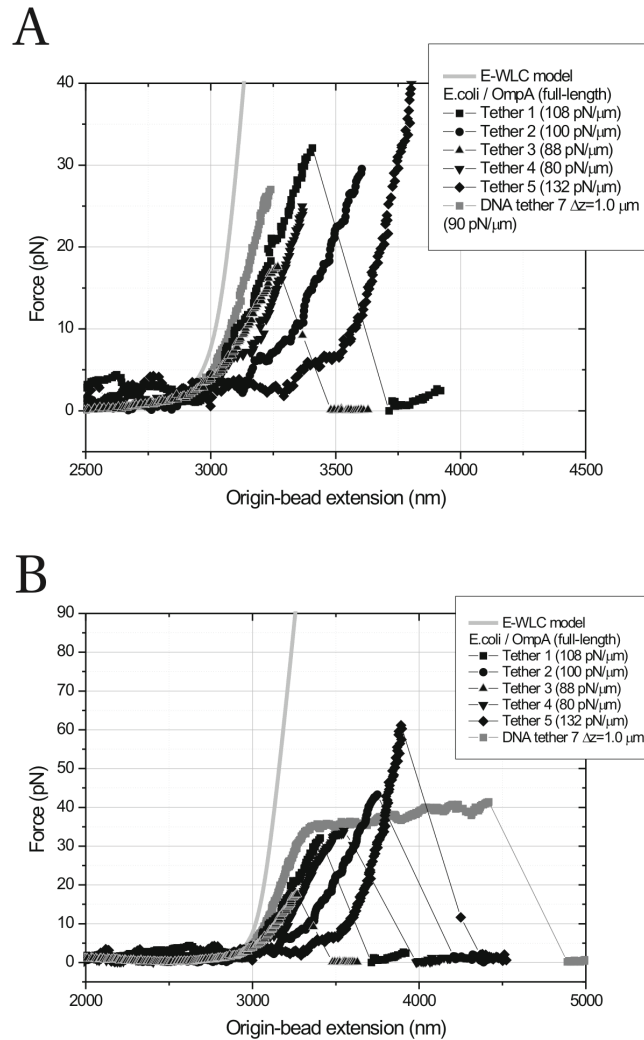
Figure 7.14. Tethers from strain MC1061 expressing full-length OmpA[SA-1]. The E-WLC model from previous curves is reproduced for comparison. The trap stiffness of the bead varied between 80 and 132 pN/μm. Pulling speed was 0.24 μm/s ("slow") for all tethers. **(A)** curves are plotted within the harmonic trap regime. **(B)** complete curves.

breaking. If $\Delta z < 1$ μm, then tube formation must occur to explain why it fits exactly the "pure" DNA tether at $\Delta z = 1$ μm and is not stiffer, as expected for $\Delta z < 1$ μm. For tether 2, similar arguments can be made: it is less stiff than "pure" DNA, it was obtained at a

(slightly) higher trap stiffness, however, onset of OS indicates a plateau force of ~45 pN, which is increased relative to the "pure" DNA curve (**Figure 7.14B**).

Apart from these two tethers, no further indication of membrane tube formation is present in these data. Also, no "long" tubes are ever seen (such as in **Figure 7.12**). Possibly, internal anchoring of the OmpA protein to the rigid PG cell wall prevents membrane tube formation.

Analysis of the measured unbinding forces at two pulling speeds

Dynamic force spectroscopy is the measurement of (single molecule) unbinding forces as a function of force loading rate. At each loading rate a distribution of unbinding forces is found. In practice, one determines the most probable unbinding force at each loading rate by fitting the distribution with a Gaussian. Assuming that unbinding is a random process, which depends on the force through Eq. 2, an expression for the most probable unbinding force *F(r)* as a function of loading rate *r* can be obtained (Evans and Ritchie 1997):

$$F = \frac{k_b T}{x_b} \ln \left(\frac{r}{k_{off}(0) \cdot \frac{k_b T}{x_b}} \right) \quad \textbf{(Equation 7.8)}$$

As we know the force at which the tethers break (the unbinding force) at two different pulling rates, we have essentially performed dynamic force spectroscopy (DFS). This allows characterization of the weakest bond within the bacterial DNA tether and thus provides information on its molecular constitution.

There are two caveats: first is that our unbinding forces, especially for the "fast" pulling rate, are most of the time outside the linear regime of the trap. As we have seen, this can either under- or over-estimate the forces. Second, tethers that unbind while in the linear trap regime, will likely underestimate the unbinding force due to additional axial bead displacements as shown earlier. Third, in conventional DFS, the loading rate is constant, whereas here, due to the DNA, the loading rate increases as the DNA molecule is stretched. Furthermore, in the force regime where tethers break (>20 pN), the typical trap stiffness (100-200 pN/μm) is comparable to that of the DNA molecule (100-500 pN/μm). The means that the loading rate (pN/s) also becomes a function of trap stiffness *k*. This can
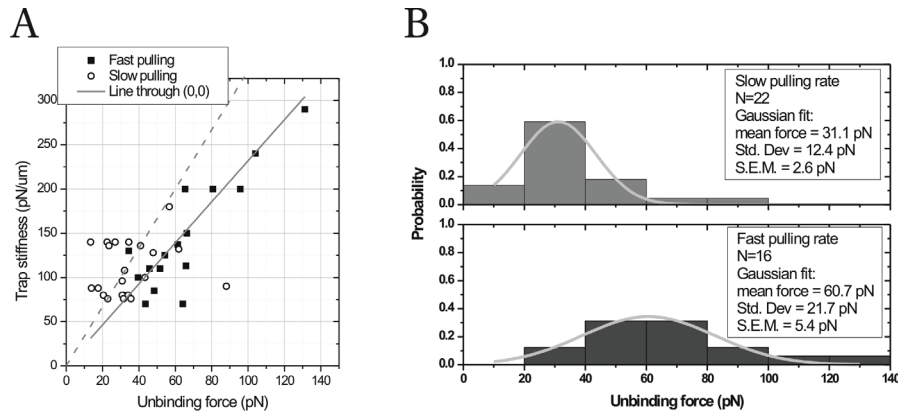
Figure 7.15. Probability distributions of unbinding forces measured at two different pulling speeds. (A) Correlation of the unbinding force with the trap stiffness. The dashed line indicates x_{bead}=300 nm and marks the end of the linear trap regime. **(B)** As both strains gave similar unbinding forces, the unbinding forces of both strains were pooled to obtain better statistics. Each histogram was fitted with a Gaussian function, giving a most probably unbinding force of 31.1±2.6 pN (SEM, N=22) and 60.7±5.4 pN (SEM, N=16), respectively. The unbinding forces are not corrected for a possible non-linear regime for high bead displacements, and the forces are lower estimates because of axial displacement of the beads, presumably resulting in a higher lateral trap stiffness (see text).

be understood as follows: when two springs are in series, the softer one will extend more than the stiffer one when the end-to-end distance is increased. Thus, for a high trap stiffness value k (stiff spring), mostly the DNA molecule "spring" is extended. If the stage is moving at a constant speed, the DNA molecule will be extended more rapidly, and will, since the force loading rate is higher, on average unbind at a higher force.

With these caveats in mind, we first plot the measured unbinding forces for the two different pulling rates as function of trap stiffness in **Figure 7.15A** (The region left of the dashed line marks the linear trap regime (x_{bead} < 300 nm)). As expected for a higher pulling rate, the unbinding forces are markedly increased. Furthermore, as expected, the measured unbinding force appears a function of trapping stiffness (the gray line is a line fit through the origin for the "fast" pulling rate). This effect should become more pronounced for higher loading rates, as for slow loading rates (low forces), the DNA "entropic" stiffness is the determining factor in the loading rate. This is exactly what we see (Coincidentally, the dashed line can be used as a guide to the eye to describe the dependence of the "slow"

unbinding forces on the trap stiffness).

The pulling rates and trap stiffness values used resulted in force loading rates of ~10-20 pN/s and 100-200 pN/s in the regime of unbinding (high forces). Dividing the unbinding force histograms by the total number of events, we end up with probability distributions to observe a particular unbinding force at the two pulling rates. In doing so, we ignore the trap stiffness spread, as these values varied over a factor two, and the pulling rate varied an order of magnitude. These probability distributions were fitted with a Gaussian function (**Figure 7.15B**). For pulling speeds of 0.24 μm/s and 2.4 μm/s, most likely unbinding forces 31.1 pN (S.E.M 2.6 pN, N = 22) and 60.7 pN (S.E.M 5.4 pN, N = 16) were found, respectively.

Discussion

OmpA-177 versus full-length OmpA

In **Figure 7.16**, bacterial tethers to both strains are plotted together, aligned at ~10 pN to compare the slopes at higher forces (> 10 pN). The F-x curves obtained on full-length OmpA are plotted in gray; those obtained on truncated OmpA (OmpA-177, "β-barrel") are plotted in black. When comparing tethers, if the F-x curve for tether A is above the F-x curve for tether B in the region F < 10 pN, and below it in the region F > 10 pN, we say that tether A is "softer" than tether B.

We find that for both strains, tethers are obtained that overlap completely with a "pure" DNA tether at Δz = 1.0 μm. Additionally, tethers are obtained that are "softer" than the "pure" DNA tether. Comparing the two strains, we find that the tethers obtained from the truncated OmpA strain are "softer" than those obtained from the full-length OmpA. This could indicate the presence of an additional compliance in these tethers, possibly through the formation of membrane tubes, as for this strain two extended tethers have been observed that were much longer than the DNA contour length.

However, there are two factors that complicate the interpretation and comparison of these curves. The first is that all tethers have been created manually, and therefore, it is not expected that Δz is exactly 1.0 μm for each curve. As demonstrated in **Figure 7.5C**, variations in Δz in the order of a few hundred nm have significant effects on the observed F-x curve. In principle, the OS plateau force, which is a function of Δz, could be used as a height indicator. However, the trap stiffness at which the curves have been obtained varies
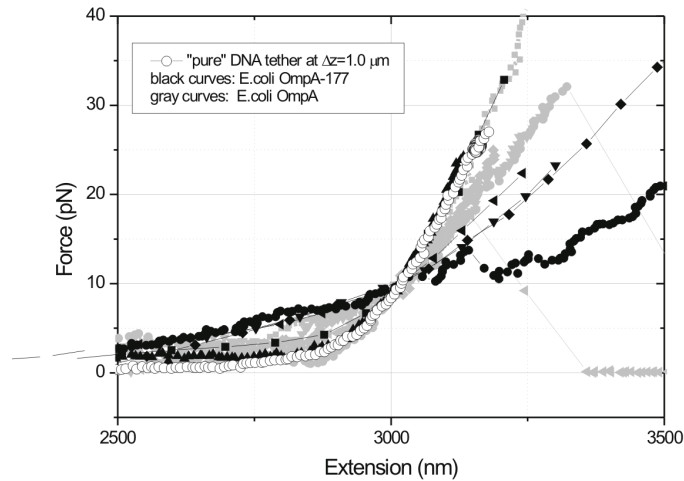
Figure 7.16. Comparison between bacterial tethers of both *E. coli* strains. The tethers were aligned to overlap at ~10 pN force. To allow comparison with "pure" DNA tethers to a stiff object, DNA tether 7 at Δz = 1.0 μm is reproduced (open circles). Evidently, from both strains can tethers be obtained that are identical to "pure" DNA. However, also "softer" tethers are obtained, for which the stiffness increases much less rapidly as the tethers are extended. For these "softer" tethers, those obtained from the strain with full-length OmpA (gray curves) appear stiffer than those obtained from the strain with truncated OmpA (black curves). A possible explanation for the softer tethers is the formation of membrane tubes, which we expect to be more easily formed from the truncated OmpA strain. At present time, we cannot exclude that the softer tethers, as well as the variation between the two strains, is caused by variations in the relative height between bacterium and trapped bead.

over a factor 2, and for some curves, the OS occurs way outside the linear regime. This is the second complicating factor. For small bead displacements beyond the linear regime, the force appears to increase more than it actually does, however, for larger bead displacements the force will likely go down. This hinders the use of the OS plateau force to rank the tethers in height.

Additional experiments, in which the relative height between bead and bacterium is carefully controlled, e.g. by using the piezo stage to create the tethers, should provide the definitive answer to whether indeed membrane tubes are formed, and if internal PG anchoring by full length OmpA reduces the probability of such tube formation. Also,

increasing the trap stiffness to e.g. 250 pN/μm will keep the bead within the linear trap regime for forces up to ~75 pN, allowing more information to be extracted from the F-x curves at high forces, such as the precise location of the OS force and the unbinding force. This is especially important for tethers obtained at the "fast" pulling rate, as the average unbinding force will be higher.

Correcting for axial displacements

We found that for our experimental geometry, the axial properties of the optical trap are important. As already mentioned, a study was reported that used a similar experimental geometry. There, a DNA molecule was tethered to a cover slip and a trapped bead, with the bead held a few μm above the surface. Force-extension curves were obtained by moving the stage and measuring the (lateral) force on the bead (Wang et al. 1997). The authors applied a geometrical model, with two main assumptions: (i) it was assumed that the lateral trap stiffness k_x did not depend on the bead's axial position. (ii) It was assumed that the axial trap stiffness k_z was related to the lateral trap stiffness via $k_x/5.9$. They obtained good agreement between the E-WLC model and their measured F-x data. We applied the same geometrical model, and found that although it brought our F-x curves more in agreement with the E-WLC model and with measured F-x curves in which axial contributions could be neglected, but that still a large discrepancy was present. This discrepancy could be resolved by assuming that over a distance of 300 nm, the lateral trap stiffness roughly doubled.

It is possible that assumption (i) does not hold for our system. We use much larger beads, which can "feel" light gradients over greater distances. Furthermore, based on visual appearance and the geometrical model, our beads are axially displaced over several hundred nm. In contrast, (Wang et al. 1997) used 520 nm PS beads, which were trapped ~290 nm above the laser focus. A force clamp was used that kept bead displacements below 60 nm from the trap center by increasing the trap stiffness (up to 400 pN/μm).

As for the second assumption, the ratio between k_x/k_z in (Wang et al. 1997), this value was based on theoretical calculations of the asymmetry of the light distribution near the focus of a focused Gaussian beam. Later experimental values measured in (Rohrbach 2005) found for a 530 nm PS bead a k_x/k_z ratio of 6.1. In the same study, it was found that the stiffness ratio k_x/k_z decreases with increasing bead diameter. The largest PS bead diameter characterized had a diameter of 1.66 μm, for which a k_x/k_z ratio of 2.7 was found.

As we used 1.87 μm PS beads, we chose to use a ratio of 2.5. However, it should be noted that this ratio likely depends on the NA of the objective, as well as the degree of overfilling.

Which unbinding force have we measured?

The molecular construct consists of a dsDNA molecule, on one end attached via multiple digoxigenin-antibody linkages to the bead, and on the other end either via one or two biotin's to one or two streptavidin molecules on the bacterial surface. Each streptavidin molecule can theoretically bind up to three SA-1 peptides, however, sterically it is unlikely that it binds more than one SA-1 peptide. Finally, the SA-1 peptide is part of the OmpA β-barrel embedded in the outer membrane.

We expect that multiple (>5) digoxigenin connections can withstand substantial amounts of force (Neuert et al. 2006). Furthermore, based on the forces required to pull out single Bacteriorhodopsin α-helices from purple membrane (100-200 pN at a force-loading rate of few 100 pN/s (Oesterhelt et al. 2000)), we also expect that pulling the complete OmpA β-barrel from the membrane requires higher forces than observed here. Thus, either the biotin-streptavidin or the (SA-1)-peptide-streptavidin complex is expected to unbind.

In **Figure 7.17**, the (two) measured unbinding forces for the bacterial DNA tethers are plotted as a function of (approximate) loading rate *r*. The error bars indicate the standard error of the mean, and therefore do not include the possible underestimation of the unbinding forces (due to axial displacement of the bead) for the "slow" pulling speed (estimated to result in a force loading rate r of ~20 pN/s), nor the under- or over-estimation (due to axial displacement, or lateral displacement outside the linear regime of the bead) of the unbinding forces for the "fast" pulling speed (~200 pN/s). The four gray curves were generated using **Equation 7.8**. For the streptavidin-biotin complex, the curve shown is the best fit through the experimental data reported in (Yuan et al. 2000), which yields a thermal off-rate of $1.67 \ 10^{-5} \ \mathrm{s}^{-1}$ and a barrier width x_b=0.49 nm. For the SA-1 peptide-streptavidin complex, *F(r)* curves were generated for three different values of x_b (0.1 nm, 0.5 nm and 1 nm) using the thermal off-rate reported in (Bessette et al. 2004).

Ignoring any possible errors in determining the unbinding forces, we find that the theoretical curve for the Streptavidin-(SA-1)-peptide complex with a barrier width of 1 nm best describes our experimental data. However, for the "slow" pulling rate, the unbinding forces are expected to be underestimated approximately a factor two, based on the DNA
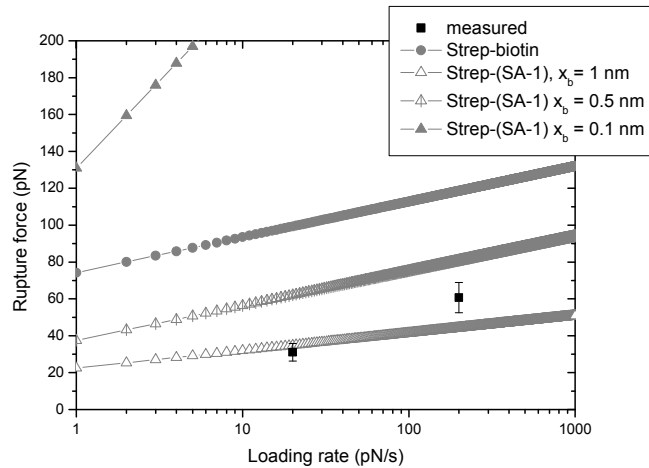
Figure 7.17. Most probable unbinding forces as a function of force loading rate. The measured unbinding forces (see also **Figure 7.15**) are plotted. The error bars indicate the standard error of the mean, and therefore do not include the possible underestimation of the unbinding forces for the "slow" pulling speed (estimated to result in a force loading rate of ~20 pN/s), nor the under- or over-estimation of the unbinding forces for the "fast" pulling speed. The four gray curves were generated using **Equation 7.8**. For the streptavidin-biotin complex, the curve shown is the best fit through the experimental data reported in (Yuan et al. 2000), which yields a thermal off-rate of $1.67\ 10^{-5}\ s^{-1}$ and a barrier width x_b=0.49 nm. For the peptide (SA-1)-streptavidin complex, F(r) curves were generated for three different values of x_b (0.1 nm, 0.5 nm and 1 nm) using the thermal off-rate reported in (Bessette et al. 2004).

overstretching experiments. Then the "true" unbinding force value will be ~60 pN, which is still almost a factor 2 less than that measured for a biotin-streptavidin bond, but would overlap with the expected value for the Streptavidin-(SA-1)-peptide complex assuming a barrier width of 0.5 nm. Therefore, these data suggest that we have measured the unbinding force of the streptavidin-(SA-1) peptide complex.

Taken together, we conclude that the bacterial tethers most likely consist of a single DNA molecule, attached to a single streptavidin bound to the SA-1 peptide displayed on the cell surface by the OmpA protein. The SA-1 peptide-streptavidin bond appears to be the weakest bond, with a most likely unbinding force of 60 pN at a loading rate of ~20 pN/s.

Materials and Methods

Preparation of DNA beads

1.87 μm carboxylated PS beads (Spherotech) were covalently functionalized with polyclonal anti-digoxigenin antibody (sheep, Roche #11333089001) using a commercial kit from Polysciences (Carbodiimide kit for carboxylated microparticles). Successful functionalization was inferred from their ability to form DNA tethers after incubation with dig-functionalized DNA. The DNA was created by PCR-ing a 300-400 bp fragment from pLexLacZ (Invitrogen) with 10% of TTP's replaced by dig-UTPs using primers DigFW and DigRV. This fragment was ligated via BglI to a BglI/AseI DNA fragment (6356 bp) from pDNR-SEAP (Clontech labs). The AseI site (overhang AT) was subsequently Klenow-filled with a nucleotide mix consisting of biotin-C14-dATP, dATP, biotin-C14-dUTP and dTTP. Thus, each DNA molecule has either 0, 1 or 2 biotin's on its end. Assuming that the dig-containing part of the DNA adheres completely to the antibody bead, and assuming a contour length/bp of 0.34 nm, the DNA tethers have an expected contour length of 2.16 μm. The DNA concentration is ~30 ng/μl. The DNA is diluted 100x in PBS, and is mixed with anti-Dig beads (The DNA concentration on the beads was tuned to give mostly single DNA tethers in a bead-bead tethering assay), washed in PBS/1% BSA to get single beads, and incubated together in a small volume (~10-20 μl) on a rotating wheel at 4C for 30 min. Finally, the beads were diluted in growth medium such that typically only a single bead would be present in the microscope's field of view. Primer sequences are available on request.

Bead tethering assay

A flow chamber is constructed by taping a Chromo-Sulfuric Acid/milliQ cleaned 24x32 mm #1 cover-slip on a thick microscope slide, depositing three parallel grease lines with a syringe and pressing a #1 18x18 mm cover-slip on top. This created a flow-cell with lanes of ~10-20 μl volume (dimensions: 18 x 4 mm x 100-200 μm). Either Streptavidin beads

(Spherotech, SVP-60-5, 6.7 μm PS) or biotin beads (Spherotech, 3.28 μm PS) were adhered aspecifically to the glass surface. Sometimes, the immobilized bead would be pulled off the surface during a force-extension experiment. It was found that the bigger the bead, the stronger the aspecific immobilization. Beads were washed three times with PBS, diluted in PBS and flowed into the chamber. Incubation was for 15 minutes at RT, then the chamber was flushed with ~5 volumes (100 μl) of PBS, turned upside-down, and further incubated for 15 min. Then the chamber was flushed with ~5 volumes (100 μl) of Defined rich glucose medium, and the sample was mounted in a sample holder, put in the setup, and an immobilized bead was searched for in the microscope. Then the sample was removed again, and either biotin-DNA beads (in case of immobilized streptavidin beads) or streptavidin-DNA beads (in case of immobilized biotin beads) were diluted in defined rich glucose medium and flowed in (~20 μl). The sample was mounted again, and a freely floating DNA bead was located. Then the microscope diaphragm was fully closed (the little light that leaks through is enough for illumination by the high NA inverted objective). The inverted objective was lowered on top of the sample until just after the diaphragm of the microscope was in focus (i.e. no Kohler illumination). This is required for trap calibration, as the red HeNe laser needs to pass through both objectives to be imaged onto the QPD. Typically, a bead was trapped at low laser power (9.5A current) and an average power spectrum was recorded. At low frequencies, (vibrational) noise obscures the bead motion, and at high frequencies, aliasing of higher frequencies obscures bead motion (the aliasing filter is not yet functional). Therefore, spectra were fit in the range 200-2000 Hz. As roll-off frequencies were typically 200-300 Hz (trap stiffness 20-30 pN/μm), this region is sufficient to obtain a good fit. Using the viscosity of water (1E-3) and the bead diameter (1.87 μm), the trap stiffness in X and Y is obtained. As the trap stiffness in X and Y direction were always the same within 10%, a single average trap stiffness value in both directions was taken. Trap stiffness values at higher laser powers were scaled linearly (see **Chapter 6**).

Bacterial tethering assay

Strain MC1061 electroporated either with pGV28 (OmpA-177[SA-1]) or with pGV33 (OmpA[SA-1]) plasmid (**Chapter 3**) was used. Cells were cultured in defined rich medium at 37°C in the presence of 0.1 mM IPTG to induce expression of OmpA[SA-1]. After growth to exponential phase (~3 hours), cells were resuspended in PBS containing 1 mg/ml BSA and incubated on ice for 10 min (blocking of aspecific sites). Then streptavidin was added (45 μg/ml) and

the cells were incubated a further 30 min on ice. Cells were pelleted twice and resuspended in PBS to wash away unbound streptavidin. At these expression levels of the SA-1 tag, pelleting results in an agglutinated clump of cells due to cross-linking by streptavidin. Vigorous pipetting then disperses the cells again. Subsequently, the cell suspension is diluted 10x into PBS and flushed into a flow chamber (volume ~20 μl, see photograph). Cells were adhered aspecifically to the (chromosulfuric acid cleaned and mQ rinsed) glass cover slip. It was found important for adhesion of cells that fresh cover slips were prepared every 2-3 weeks. After 15 min, the flow chamber is flushed with 5 volumes of PBS (~100 μl) and turned upside-down. After another 15 min, the flow chamber was flushed again, now with ~5 volumes of defined rich medium. The beads were diluted in growth medium such that typically only a single bead would be present in the microscope's field of view. The trapping laser current supply, and the HeNe position detection laser were turned on 3 hours in advance to stabilize the beams. A tether is formed by reducing the laser power on a trapped DNA bead, positioning the bead above the bacterium and subsequently reducing the z-distance between trap and bacterium (pressing the bead on top of the bacterium), and waiting a few seconds. Then the trap-bacterium distance is increased again manually until the bead has returned to the zero-force z-position, the laser power is increased and the stage is moved away at a constant speed (either 2.4 or 0.24 μm/s) in either X or Y direction, depending on which direction gives an angle closest to a right angle with the long axis of the cell.

Data analysis

The bacterial tethers were analyzed as follows. The tethering events was recorded at 25 Hz with a DVD recorder and burned on DVD as a collection of 20-30 1-2 minute movies. With an IDL program developed at AMOLF (Track_bead), for each movie, the positions of the bead and stage are tracked with sub-pixel resolution using a cross-correlation algorithm based on a template (portion of an) image. As template used for bead tracking, typically a frame is chosen containing the bead right after the tether broke, as this frame represents the bead position without force acting on it. The stage was tracked either via a bead that was attached (preferred option), or via an additional bacterium attached, or via the bacterium being tethered (least preferred option) depending on what was present in the field of view. Pixel sizes for the camera and objective used (Kappa CF 8/4 DX together with water objective at 1.5X magnification) were determined using the piezo-stage, by moving a

bead stuck on the surface in X and Y steps of 1 μm over the surface and video tracking the positions. We found pixel sizes in X and Y of 93.8 nm and 85.4 nm, respectively. The text files containing the pixel values were subsequently manipulated and plotted in Origin. The stage positions were shifted manually such that the stage position in the frame just before stage translation starts was (0,0). The bead positions were shifted manually such that right after a tether breaks the bead is at (0,0). We defined the tether extension length as x_{stage}-x_{bead}. Defined in this way, the bead radius is part of the tether extension, and we assume that the tether is attached on the bacterium exactly underneath the center of the bead. The magnitude of the force vector on the bead was obtained by multiplying the length of the bead position vector (x_{bead}, y_{bead}) with the trap stiffness obtained from an average power spectrum as described above. Plotting the force magnitude as a function of tether extension length yields a force-extension (F-x) curve. The DNA tethers between beads were analyzed in the same way, except that the immobilized bead was tracked for the stage position, and arbitrarily shifted on the X-axis, as the absolute tether extension is not known, only the increase in tether extension since the measurement started.

The force vector was plotted in the video images by the following steps. The DVD movies were re-played and grabbed by an analog video grabber at 40 ms/frame (Silicon Graphics PC, Anaconda) using an IDL program (grabber_program) that writes the grabbed images as a tiff stack. Using a second IDL program (track_bead), the tiff stacks were tracked for the bead position, and care was taken to get the center of the bead template as close to the bead center. The tracked coordinates now indicate the bead position as pixel values. A small routine was written in IGOR that needs as manual input the frame where the force on the bead is zero (usually the last frame), and then writes in each frame the vector between the zero force bead position and the current bead position as a white line that is proportional in length to this distance (and thus can be interpreted as a force vector).

These movies were used to more accurately determine the anchoring point on the bacterium: in ImageJ, the pixel coordinates of the trapped bead at t=0 (onset of stage motion) are estimated. Then, the frame right before the tether breaks is used to get the intersection of the force-vector and the bacterium. A straight line crossing this point, and parallel to the pulling direction was drawn, and the frame at t=0 is displayed again. The pixel coordinates of the point where this line intersects the bacterium was then estimated,

and the difference in pixel values was used to shift the tracked stage position (starting at 0,0).

To visualize the force vectors in the reference frame where the bacterium does not move, the tracked-stage data from the f-x curves was used. The pixel size calibration constants were determined for the re-played grabbed video data by using a movie in which a bead stuck to the stage was displaced in X and Y in steps of 1 μm.